

## Perspective

## Micro-hydrogel injectables that deliver effective CAR-T immunotherapy against 3D solid tumor spheroids

Anisha B. Suraiya<sup>a,b</sup>, Vera J. Evtimov<sup>b</sup>, Vinh X. Truong<sup>a,1</sup>, Richard L. Boyd<sup>b</sup>, John S. Forsythe<sup>a</sup>, Nicholas R. Boyd<sup>b,\*</sup>

<sup>a</sup> Department of Materials Science and Engineering, Monash Institute of Medical Engineering, Monash University, Clayton, Victoria 3800, Australia

<sup>b</sup> Cartherics Pty, Ltd., Clayton, Victoria 3168, Australia

## ARTICLE INFO

## Keywords:

Microgels  
Cell encapsulation  
Immunotherapy  
CAR-T cells  
Cell delivery  
Tumor spheroids

## ABSTRACT

Chimeric antigen receptor (CAR-) T cells are revolutionizing cancer treatment, as a direct result of their clinical impact on the treatment of hematological malignancies. However for solid tumors, CAR-T cell therapeutic efficacy remains limited, primarily due to the complex immunosuppressive tumor microenvironment, inefficient access to tumor cells and poor persistence of the killer cells. In this *in vitro* study, an injectable, gelatin-based micro-hydrogel system that can encapsulate and deliver effective CAR-T therapy is investigated. CAR-T cells targeting TAG-72, encapsulated in these microgels possessed high viability (> 87%) after 7 days, equivalent to those grown under normal expansion conditions, with retention of the T cell phenotype and functionality. Microgel recovered CAR-T cells demonstrated potent on-target cytotoxicity against human ovarian cancer *in vitro* and on three-dimensional tumor spheroids, by completely eliminating tumor cells. The gelatin-based micro-hydrogels have the potential to serve as carrier systems to augment CAR-T immunotherapeutic treatment of solid tumors.

## Introduction

Chimeric antigen receptor (CAR-) T cell-based immunotherapy employs genetically modified T cells to express synthetic antibody molecules capable of recognizing specific antigens present on the surface of tumor cells [1,2]. The therapy has proven its clinical success in treating liquid tumors like acute lymphoblastic leukemia (ALL) [3,4]. However, the clinical application of CAR-T cells to solid tumors is limited mainly due to the lack of identification of unique tumor-associated antigen(s), inefficient trafficking of T cells to the tumor site, their poor retention and failure to overcome the immunosuppressive tumor microenvironment (TME) [5–7]. Moreover, various cells and their mediators play an important role in tumor-stroma interactions [8,9].

Cancer-specific antigens coupled with their limited expression on healthy tissue is required for successful on-target CAR-T therapy [10]. One such molecule is the oncofetal tumor-associated glycoprotein-72 (TAG-72) which is highly expressed in epithelial ovarian cancer [11], and most adenocarcinomas including breast [12], prostate [13] and colorectal cancer [14]; whilst expression in normal adult tissues is rare

[15]. In ovarian cancer, owing to the lack of early diagnostic markers and clinical symptoms, most cases are diagnosed at advanced stages when it has already spread through the peritoneal cavity [16]. CAR-T cell based immunotherapy could provide a more targeted therapeutic approach for the treatment of ovarian cancer. Herein, the CAR-T cells are targeted against TAG-72, however efficient delivery of CAR-T cells to the specific tumor site remains a challenge. In order to obtain effective clinical outcomes, doses of CAR-T cells typically in the range of  $10^8$ - $10^9$  are required [17,18]. Higher doses of CAR-T cells attacking cancer can induce cytokine storm syndrome where high amounts of cytokines are released into the bloodstream, causing extreme fever and can even lead to neurotoxicity and death [19,20]. These are a major safety risk for the patient irrespective of therapeutic potential. Also, it is important to determine the cytokines in various tissues during immunotherapy by utilising different techniques [21]. Collectively, these factors limit the potential clinical efficacy of CAR-T cells to solid tumors and need to be addressed.

Biomaterials-based delivery platforms can offer a localized and controlled release of “cargo” at the TME while providing a protective

\* Corresponding author.

E-mail address: [nicholas.boyd@hudson.org.au](mailto:nicholas.boyd@hudson.org.au) (N.R. Boyd).

<sup>1</sup> Present address: School of Chemistry and Physics, Queensland University of Technology, Brisbane, Queensland 4000, Australia.

environment for the CAR-T cells enabling their proliferation [22,23]. For example, an alginate-based porous scaffold functionalized with adhesion molecules and stimulatory signals was developed to deliver tumor-reactive T cells to the tumor site [22]. These scaffolds, when implanted in a mouse model of breast cancer resection completely prevented tumor relapse compared to intravenously administered T cells and those directly injected at the resection cavity. Although scaffold-based implants can be beneficial in locally delivering immune cells and to effectively boost the *in vivo* persistence in the TME, such methods are invasive, necessitating surgery for implantation. Therefore, injectable systems are preferred over scaffolds for localized immune cell delivery.

Utilizing injectable and cell-laden hydrogel microstructures (microgels) is a promising approach to address some of the challenges associated with localized cell delivery. We have previously demonstrated the use of these biocompatible gelatin-based microgels as a three-dimensional (3D) culture platform for *in vitro* T lineage induction and thymic epithelial cell maintenance [24]. Our approach implements a pipette-tip based microfluidic device in conjunction with a biorthogonal photo click reaction for the crosslinking of norbornene functionalized gelatin and thiol modified poly(ethylene glycol) (PEG) [24–26]. Herein, we investigate the capacity for the microfluidic microgels to serve as an injectable vehicle for the delivery of CAR-T cells. Since two-dimensional (2D) monolayer cultures do not recapitulate the complexity of the TME [27,28], here we utilized 3D solid tumor spheroids to better mimic the physiological tumor niche and to study the cytotoxic potential of CAR-T cells. These cell-laden microgels could potentially be injected into the peritoneal cavity of patients with metastatic ovarian cancer for the delivery of CAR-T cells at the tumor site with enhanced persistence. Our strategy has the potential to reduce the dose size per injection, thereby reducing the manufacture fail rate for patients with depleted immune systems. Our strategy also has the capacity to reduce the likelihood or severity of cytokine storm syndrome through the sustained release of CAR-Ts during degradation of the microgels *in vivo*.

## Experimental section

### Hydrogel precursor synthesis

Norbornene functionalized gelatin (GelNB) was synthesized via a two-step process based on our previously published protocols [24,25] as detailed in the supplementary information. Briefly, 5-norbornene-2-carboxylic acid dissolved in dichloromethane (DCM) was first functionalized with N-hydroxysuccinimide (NHS) and N-(3-(dimethylamino)propyl)-N'-ethylcarbodiimide hydrochloride (EDC-HCl) to generate an amine-reactive ester. This intermediate product was subsequently mixed with gelatin in a solution of N,N-dimethylformamide (DMF)/water (1:1 v/v), followed by purification via dialysis. Finally, the solution was lyophilized to obtain norbornene-conjugated gelatin. Thiol modified linear PEG (PEG(SH)<sub>2</sub>) was synthesized via a three-step route based on our previously reported protocol [26,29].

### Photorheology

Rheological analyses of hydrogels were conducted on a parallel plate rheometer (Anton Paar Physica MCR 501) using a top plate of diameter 12 mm. Time sweep measurements were conducted at a strain of 1% and a frequency of 1 Hz. A bottom quartz plate connected to a light guide was used to transmit light. Hydrogel prepolymers were prepared from stock solutions to obtain a final mixture with concentrations of GelNB (4% w/v), PEG(SH)<sub>2</sub> (1% w/v), and photoinitiator, lithium phenyl-2,4,6-trimethylbenzoylphosphine (LAP) (0.03% w/v; Tokyo Chemical Industry, Japan). The final prepolymer mixture (50  $\mu$ L) was placed on the bottom plate and the top plate was extended to a gap size of 0.3 mm. The solution was let to stabilize for 2 min and then photopolymerization was induced by light irradiation (400–500 nm, 10 mW/cm<sup>2</sup>, 10 min)

using a UV lamp (OmniCure S2000, Lumen Dynamics).

### Microfluidic device fabrication and generation of microgels

A pipette tip-based microfluidic device was used for the generation of microgels [24–26]. Briefly, for the fabrication of the device, first, a moldable glue was inserted within a 200  $\mu$ L pipette tip to form the device chamber and two parallel inlets were made within the chamber using two polytetrafluoroethylene (PTFE) tubes (ID: 0.3 mm, OD: 0.76 mm; Cole-Parmer). The mold was left to cure for 48 h to form channels, followed by the removal of the pipette tip and the PTFE tubes. In these channels, two new PTFE tubes (15 cm) were inserted; one for oil and the other for hydrogel prepolymer solution. In the next step to make a nozzle, a 0.5 mm hole was made in a silicon tube (ID: 0.5 mm, OD: 1.3 mm; Gecko Optical, Australia) using a biopsy punch (OD: 0.5 mm), followed by inserting the tube in a pipette tip. Then, the outlet end of the PTFE tube for the hydrogel solution was attached to the silicon tube adjacent to the punched hole. The pipette tip was then moved up towards the mold to close the chamber. Finally, two 25G needles were separately inserted into the inlet ends of the PTFE tubes to administer the oil and the hydrogel solution.

For the generation of microgels, hydrogel prepolymers (500  $\mu$ L) were prepared as described in the photorheology section. Gel suspension and microfluidic oil (Picosurf, 2% in FC-40) taken in separate syringes were connected to the microfluidic device, followed by loading in separate syringe pumps with flow rates set at 1 mL/h for the aqueous phase and 4 mL/h for the oil phase. Pre-cured microgel droplets dispersed in oil were photopolymerised by light irradiation (400–500 nm, 10 mW/cm<sup>2</sup>, 10 min) using a UV lamp. Microgels retrieved from oil were washed and redispersed in Dulbecco's phosphate-buffered saline (DPBS)/media.

### Cell culture

#### Cancer cell lines

Cell lines were purchased from American Type Culture Collection (ATCC, USA). Human ovarian adenocarcinoma cell line OVCAR3 was cultured in RPMI-1640 (Sigma-Aldrich, USA) with fetal bovine serum (FBS) (20% v/v, Bovogen, Australia), bovine insulin (0.01 mg/mL, Sigma-Aldrich, USA), and penicillin-streptomycin (1X, Pen/Strep, Gibco, USA). Human breast cancer cell line Hs578T was cultured in Dulbecco's Modified Eagle's Medium (DMEM) (Gibco, USA) with FBS (10% v/v), bovine insulin (0.01 mg/mL), and Pen/Strep (1X).

#### CAR-T cells

T cells transduced to express anti TAG-72 CARs (hereafter referred to as  $\alpha$ TAG-72 CAR-T cells) were developed by Cartherics Pty Ltd [30]. Peripheral blood mononuclear cells (PBMCs) were isolated from whole blood obtained from consenting, healthy donors (Australian Red Cross, Monash Health HREC number 16055A) after informed consent. Briefly, PBMCs were isolated via Ficoll-Paque (GE Healthcare, USA) density gradient centrifugation using Leucosep tubes (Greiner Bio-One, Austria). T cells were sorted from PBMC fractions and activated via anti-CD3/anti-CD28 magnetic beads (DynaBeads, ThermoFisher Scientific, USA) as per the manufacturer's instructions. Beads were removed immediately before the addition of TAG-72 lentiviral CAR construct [30] and transduction occurred over 48 h in media containing IL-2 (Miltenyi Biotec, Germany). Removal of the virus via centrifugation ensues, and cells were transferred to a complete T cell medium comprising TexMACS Medium (Miltenyi Biotec, Germany), human AB serum (5% v/v, Sigma Aldrich, USA), human platelet lysate (5% v/v, Cook Regentec, USA) supplemented with human IL-2, IL-7, IL-15 and IL-21 (Miltenyi Biotec, Germany). On day 10 post-transduction CAR+ cells were isolated based on GFP expression using MACSQuant Tyto Cell Sorter (Miltenyi Biotec, Germany). CAR+ cells were harvested, washed and resuspended in Tyto Buffer containing Viability Dye 405/452 (Miltenyi Biotec, Germany) and incubated in ice for 15 min protected

from light. Following washing and collection via centrifugation, the cells were resuspended in Tyto Buffer to achieve a final density of  $2-4 \times 10^6$  cells/mL. Following sorting, cells were transferred to complete T cell medium for continued expansion. Activated, non-transduced (NT) T cells (no CAR) were maintained in parallel and analyzed for all donors.  $\alpha$ TAG-72 CAR-T cells and NT T cells were maintained in the complete T cell medium at a density of  $1 \times 10^6$  cells/mL at  $37^\circ\text{C}$  with 5%  $\text{CO}_2$ .

#### CAR-T cell encapsulation in microgels

The microfluidic device and associated equipment were UV sterilized for 30 min in a biosafety cabinet before cell encapsulation studies. Filter sterilized microfluidic oil was loaded in one of the syringe pumps. Pre-activated  $\alpha$ TAG-72 CAR-T cells in suspension cultures were spun down at 300 g for 5 min, resuspended in 1 mL complete media, and counted using a MUSE Cell Analyser (Merck, Germany). The pre-polymer solution (500  $\mu\text{L}$ ) was diluted in complete media with cells at a density ranging from  $1-5 \times 10^6$  cells/mL and loaded in the aqueous phase syringe. Cell encapsulated microgels were generated as detailed in the microfluidic device fabrication section. CAR-T cells containing micro-particles were thoroughly washed in media and resuspended in fresh complete T cell media followed by incubation at  $37^\circ\text{C}$  and 5%  $\text{CO}_2$ . Media were replenished every two days until analysis.

#### Cell viability and 3D cell distribution analysis

Cell viability and distribution of T cells within the microparticles were visually analyzed by live/dead confocal microscopy. Live/dead staining (Thermo Fisher Scientific, USA) and imaging were conducted on day 1 and day 7 post encapsulation. Microgels removed from culture media were washed in DPBS and incubated in a live/dead solution (DPBS comprising 0.5  $\mu\text{L}/\text{mL}$  calcein-acetoxymethyl ester (AM) and 2  $\mu\text{L}/\text{mL}$  ethidium homodimer-1) for 20 min. The viability and 3D distribution of CAR-T cells in different focal planes were analyzed by confocal microscopy (Nikon C1 inverted microscope, Japan) capturing Z-stack images through a depth of 500–600  $\mu\text{m}$ . Quantitative measurement of cell viability was performed by counting live and dead cells in five microgels at each time point using ImageJ software (NIH, USA) and cell viability was calculated as the ratio of live cell number to the total cell number.

#### Phenotypic analysis of $\alpha$ TAG-72 CAR-T cells pre and post microgel encapsulation

The phenotype of CAR-T cells prior to microgel encapsulation was analyzed via flow cytometry. Cells grown in suspension cultures and those exposed to the same intensity of light used to induce photopolymerization of microgels were also used as controls to study the effect of microgel fabrication on cell state. CAR-T cells stained in either an antibody cocktail (Table S1) or relevant isotype control, where cells were incubated for 10 min at  $4^\circ\text{C}$ . Cells were washed once by centrifugation at 300 g for 5 min. Finally, cells were resuspended in buffer (DPBS comprising 0.1% bovine serum albumin (BSA) and 5 mM ethylenediaminetetraacetic acid, (EDTA)) and propidium iodide (PI) was added as viability indicator just before flow cytometric analysis using a MACSQuant Analyzer 10 (Miltenyi Biotec, Germany). Data was analyzed using FlowLogic software (Inivai Technologies, Australia). Prior to phenotype analysis, gates were set to exclude doublets, debris, and dead cells.

The effect of microgel encapsulation on the phenotype of CAR-T cells was studied by recovering encapsulated cells from microgels on day 7 via enzymatic digestion using 1X Collagenase-IV (Life Technologies, USA) for 20 min. Flow cytometric analysis was performed as described above.

#### TAG-72 expression in cancer cell lines

Expression of TAG-72 in cancer cell lines OVCAR3 and Hs578T was

analyzed using flow cytometry. Cells were stained using anti TAG72-AVP04 (Avi pep, Australia) at 1/20 dilution, incubated for 10 min at  $4^\circ\text{C}$ , washed once before resuspension in PI. Cells were gated based on the scatter profiles to identify intact, single cells. Viable (PI negative) cells were then selected for, prior to analyzing surface marker expression.

#### Real-time in vitro cytotoxicity analysis of microgel recovered CAR-T cells

*In vitro* CAR-T cell killing assays were performed using a real-time cell analysis (RTCA) instrument (xCELLigence RTCA SP- Analyzer, ACEA Biosciences, USA). Microgel encapsulated CAR-T cells recovered via enzymatic digestion on day 7 post encapsulation were used as effector cells. OVCAR3 and Hs578T cancer cell lines were used as target cells and were seeded at 10,000 cells/well in an electronic 96 well plate (ACEA Biosciences, USA) having gold microelectrodes on its bottom surface. Change in impedance was monitored every 15 min for at least 6 h prior to the addition of effector cells and represented as 'cell index'. The recovered T cells were incubated for 24 h in IL-7 (5 ng/mL) containing medium to reduce activation and hence the degree of non-specific killing. Microgel recovered/control  $\alpha$ TAG-72 CAR-T cells and NT T cells were used as effectors at 5:1 effector to target (E:T) ratio [30] and cell index was measured for 24 h. Values were normalized to the time from the addition of CAR-T cells and analysis was performed using GraphPad Prism 8.0 software.

#### Establishment of 3D tumor spheroid culture

3D tumor spheroids of OVCAR3 were developed via adapting similar previously published methods with appropriate modifications [31,32]. Briefly, cancer cells trypsinized from culture flasks were resuspended in serum-free tumorsphere medium (MammoCult, STEMCELL Technologies, USA) supplemented with heparin (4  $\mu\text{g}/\text{mL}$ , STEMCELL Technologies, USA), hydrocortisone (0.48  $\mu\text{g}/\text{mL}$ , STEMCELL Technologies, USA) and Pen/Strep (1X). Cells were seeded at a density of  $5 \times 10^3$  cells/well in 50  $\mu\text{L}$  in 96 well Ultra-Low Attachment plates (Corning, USA) and cultured for 14 days to enable the formation of spheroids. Media was changed every four days in a gentle manner without disturbing the floating spheroid cultures. Spheroids with well-defined boundaries were observed by 2 weeks. Tumorspheres with defined borders and size  $\geq 40 \mu\text{m}$  were counted on day 14 of culture from 24 wells in each group, and tumorsphere formation efficiency (TFE) was calculated using the following equation:

$$TFE (\%) = \frac{\text{Number of tumorspheres per well}}{\text{Number of cells seeded per well}} \times 100$$

#### 3D spheroid CAR-T cell cytotoxicity assay

##### Real-time imaging: SNARF-1 and CSFE staining

For time-lapse imaging of 3D tumor spheroid killing using CAR-T cells, OVCAR3 tumorspheres were fluorescently tagged with SNARF-1 (ThermoFisher Scientific, USA) and CAR-T cells were labeled using CSFE (ThermoFisher Scientific, USA). For SNARF-1 staining, day 14 tumorspheres cultured in low adhesion 96 well plates were pooled from 3 wells and placed on each well of 8 well chamber slides one day before imaging. For 2D OVCAR3 control well,  $4 \times 10^4$  cells were seeded and kept at  $37^\circ\text{C}$  incubator overnight. OVCAR3 spheroids were labeled with SNARF-1. Media was carefully aspirated off from the sides of the well, following a PBS wash 200  $\mu\text{L}$  of SNARF-1 (20  $\mu\text{M}$ ) working stock was added and incubated for 30 min at  $37^\circ\text{C}$ . After the incubation period, the stain was removed and fresh media was added.

T cells were stained using CSFE (100 nM) staining solution. Briefly, NT control T-cells and  $\alpha$ TAG-72 CAR-T cells, grown in both suspension culture and recovered from microgels, were counted using MUSE analyzer, centrifuged at 300 g for 5 min and the supernatant was

discarded. CFSE staining solution was added to the pellet and incubated for 10 min at 37°C. Followed by the addition of complete media to quench the stain, cells were spun down and resuspended at  $1 \times 10^6$  cells/mL in complete media. 200  $\mu$ L cell suspension of control  $\alpha$ TAG-72 CAR-T cells, NT T cells and cells recovered from microgels was added to the respective wells.

Real-time images were captured every 15 min for 15 h using Olympus FV1200 confocal microscope in bright field, TRITC and FITC channels. Images were overlaid from the three channels, and time-lapse video was generated by stitching together images via FIJI software.

#### Flow cytometric analysis of 3D spheroids and CAR-T cells

To analyze the 3D spheroid killing ability of microgel recovered

CAR-T cells, cells were recovered from microgels 7 days post encapsulation and transferred to IL-7 containing media.  $\alpha$ TAG-72 CAR-T cells and NT T cells were added at  $5 \times 10^4$  cells/well to OVCAR3 tumorspheres and incubated at 37°C. After four days of co-culture, cells were dissociated mechanically (ejecting via a 25G needle attached to a syringe) and enzymatically (Tryple, 10 min at 37°C) (ThermoFisher Scientific, USA) into a single-cell suspension and prepared for flow cytometric analysis (described in section: Phenotypic analysis of  $\alpha$ TAG-72 CAR-T cells). OVCAR3 cells were gated by the expression of EpCAM and T cells were identified by the expression of CD3 (Table S2).

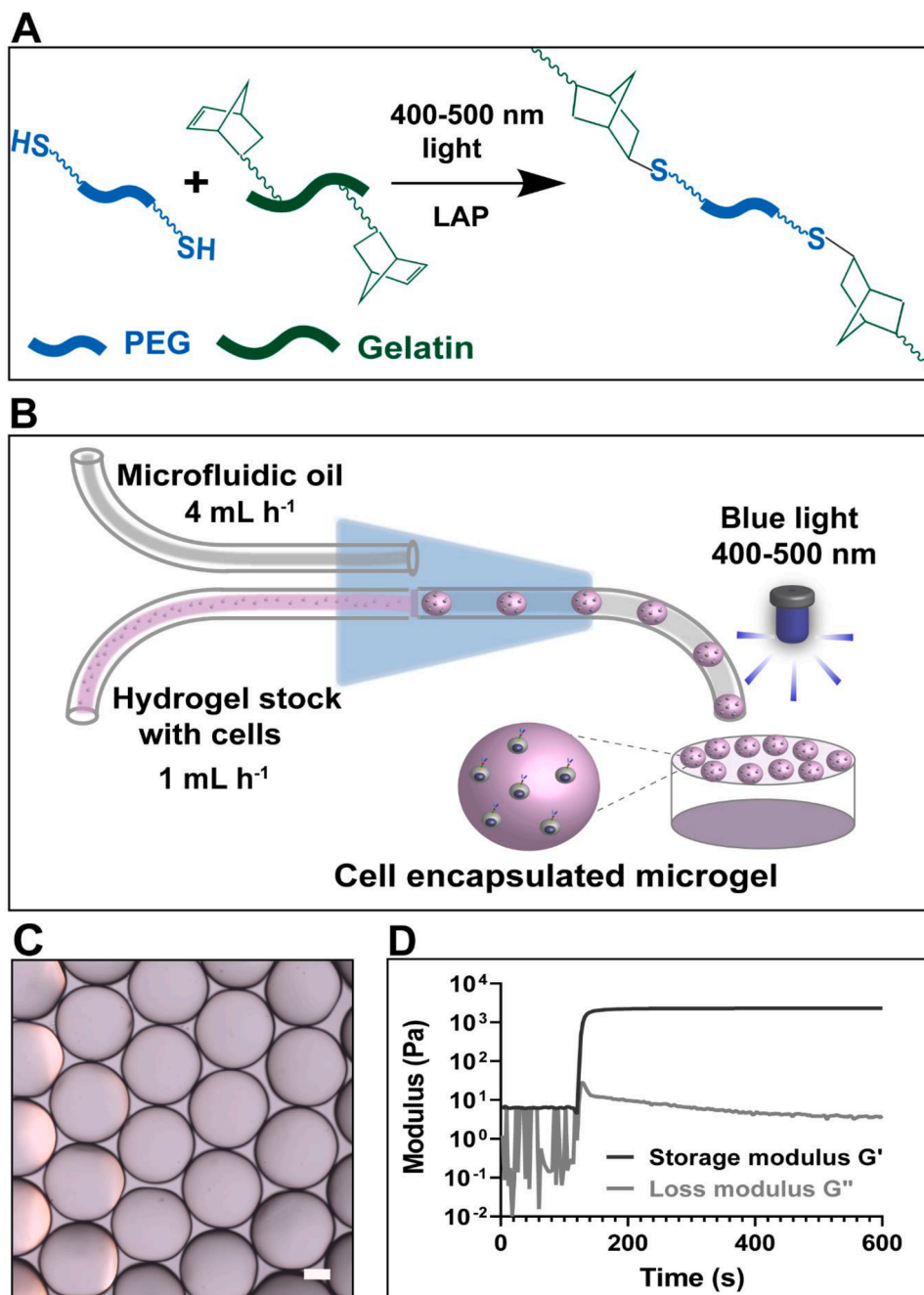


**Fig. 1.** Microgel generation and hydrogel characterization (A) Simplified scheme of the thiol-norbornene photoclick reaction between thiol-functionalized linear PEG and norbornene-functionalized gelatin. (B) Schematic illustration of pipette-tip based microfluidic device and microgel generation. (C) Bright-field image of photoreacted microgels in oil (scale bar represents 200  $\mu$ m). (D) Photoreology measurements of storage and loss moduli.

### Statistical analysis

Statistical analysis was performed using GraphPad Prism 8.0 software. All values presented are mean  $\pm$  standard deviation (SD). Biological triplicates were used throughout unless otherwise stated. For cell viability measurements unpaired t-test with Welch's corrections was conducted. The population frequency of T cell markers was analyzed by one-way ANOVA with Bartlett's test and Tukey's post hoc test. For the proportion of cancer cells in spheroid cultures, unpaired (nonparametric) t-tests with Welch's correction were performed. A p-value  $<0.05$  was considered statistically significant (\*p  $<0.05$ , \*\*p  $<0.01$ , \*\*\*p  $<0.001$ , \*\*\*\*p  $<0.0001$ ).

## Results and discussion

### Microgel generation and hydrogel characterization

Microgels were generated using a pipette-tip based microfluidic device utilizing norbornene functionalized gelatin and thiol functionalized PEG via a visible light-mediated thiol-ene click reaction (Fig. 1A & B) [24–26]. Microgel size can be altered on demand by varying the tube diameter or flow rate of the aqueous/oil phase [25]. In this study, microgels of diameter in the range of 600  $\mu\text{m}$  were obtained (Fig. 1C). Gelation kinetics of the hydrogel was assessed using photorheology and gelation occurred rapidly after light irradiation, determined by the cross-over of storage modulus ( $G'$ ) and loss modulus ( $G''$ ). Following light exposure storage modulus initially increased and plateaued at around 2000 Pa (Fig. 1D).

### CAR-T cells encapsulated in microgels are viable and retain phenotype pre- and post *in vitro* culture

Live/dead viability analyses of  $\alpha\text{TAG-72}$  CAR-T cells encapsulated in microgels at  $3 \times 10^6$  cells/mL have shown high viability on day 1 and day 7 post encapsulation. Cells at lower densities have displayed reduced viability, potentially due to the lack of adequate cell-cell interaction and higher cell concentrations tend to clog the microfluidic system (data not shown). Therefore,  $3 \times 10^6$  cells/mL were used for encapsulation studies and cells displayed higher viability on day 1 ( $83 \pm 2\%$ ) (Fig. 2A, B) demonstrating the biocompatibility of the system. Viability on day 7 post encapsulation was  $88 \pm 1\%$ , with uniform distribution of cells within the microgels, indicating the suitability of microgels for sustained culture periods and adequate media transport through the gels of cytokines necessary for T cell survival. The number of cells per microparticle on day 1 was  $164 \pm 26$  and on day 7 was  $239 \pm 35$  ( $n = 5$ ). This modest increase in T cell number is indicative of possible proliferation within the microgels. Whilst there is expected system dependency, a recent study investigating hyaluronic acid-PEG based hydrogels conjugated with stimulatory signals as an artificial T cell-activation matrix enabled proliferation of CD8+ T cells [33]. Another study using a thermoresponsive hydrogel for the 3D culture of T cells and *in vivo* cell delivery has shown a significant expansion of pre-activated T cells *in vitro* and gradual migration of cells from the gel following subcutaneous injection in mice [34]. These studies have displayed the potential of hydrogels to improve T cell therapy strategies. In our study, cell viability assays demonstrated the survival and maintenance of  $\alpha\text{TAG-72}$  CAR-T cells in microgels, showing their feasibility as carrier systems of CAR-T cells.

Flow cytometry analysis of CD4/CD8 (T cell markers), CD69 (activation marker [35]) and PD-1 (T cell negative regulator [36]) of CAR-T cells released from microgels indicated that cells retain full and normal functional receptors, unchanged by microgel encapsulation (Fig. 3). A CD4/CD8 ratio of 1.5–2.5 is generally considered normal; however, other factors like age, gender or genetics may affect this ratio [37] therefore, variations will be observed with different donors. In our study, a significantly higher percentage of CD4 cells to CD8 cells could

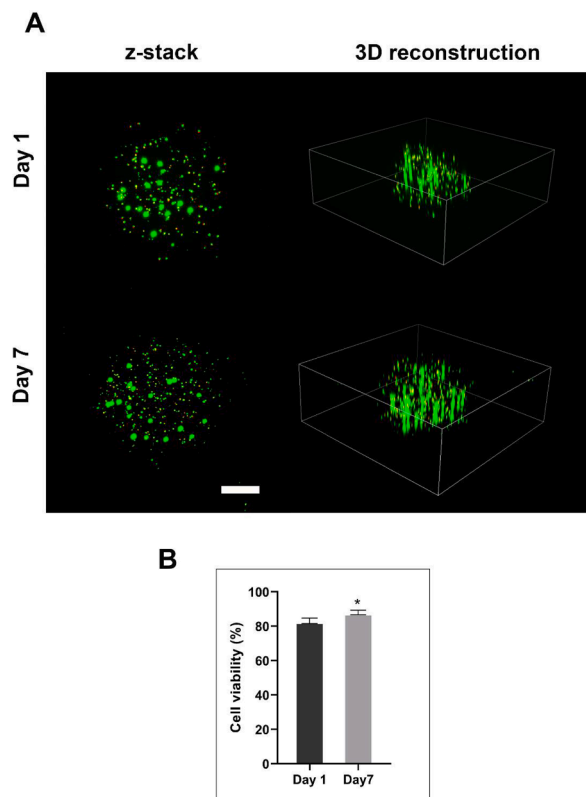


**Fig. 2.**  $\alpha\text{TAG-72}$  CAR-T cell encapsulation in microgels (A) Viability of  $\alpha\text{TAG-72}$  CAR-T cells encapsulated in microgels following 1 and 7 days of encapsulation. Live cells are stained green using calcein-AM and dead cells are stained red using ethidium homodimer. Scale bar represents 200  $\mu\text{m}$ . (B) Quantitative analysis of  $\alpha\text{TAG-72}$  CAR-T cell viability in five different microgels at each time point ( $n = 5$ ) (\*p  $<0.05$ ).  $\alpha\text{TAG-72}$  CAR-T cell: T cells transduced to express anti TAG-72 CARs.

be attributed to the expansion conditions favoring CD4 cells (Fig. 3A–E). Nevertheless, there was no change in the CD4/CD8 expression seven days post microgel expansion (Fig. 3C–E) compared to cells grown in suspension culture. Notably, the expression of activation marker CD69 in different culture conditions was inherently high and was not negatively impacted by encapsulation (Fig. 3F). PD-1 was characterized to provide an indication for T cell exhaustion [38] and there was no substantial expression of PD-1 in any of the culture conditions (Fig. 3G). The CAR expression also remained unaffected post microgel encapsulation (Fig. 3C, H). Cells exposed to blue light also had no significant effect on phenotype (data not shown). Collectively, these findings validate the applicability of these gels as culture vessels for CAR-T cells.

### Microgel recovered CAR-T cells demonstrate on-target cytotoxic function against TAG-72 ovarian cancer cells in 2D *in vitro* setting

Prior studies have shown the expression of TAG-72 in patient samples of ovarian cancer [16,39] and various ovarian cancer cell lines [40, 41]. OVCAR3 cell lines are reported to present higher expression of TAG-72 [30,40]. Although this present study mainly focuses on ovarian cancer cells, hydrogel augmented CAR-T immunotherapy can in principle be applied to a variety of solid tumors. Accordingly, the surface expression of TAG-72 on two epithelial-type cancer cell lines demonstrated the suitability for each to be targeted by  $\alpha\text{TAG-72}$  CAR-T cells. With reference to Jurkat cells as high TAG-72 positive controls [42] and PBMC T cells as negative controls (data not shown), the phenotypic analysis confirmed a comparatively high TAG-72 expression in the ovarian cancer cell line OVCAR3 and lower expression in the breast cancer line Hs578T cells (Fig. 4A). Whilst OVCAR3 cells appeared to be

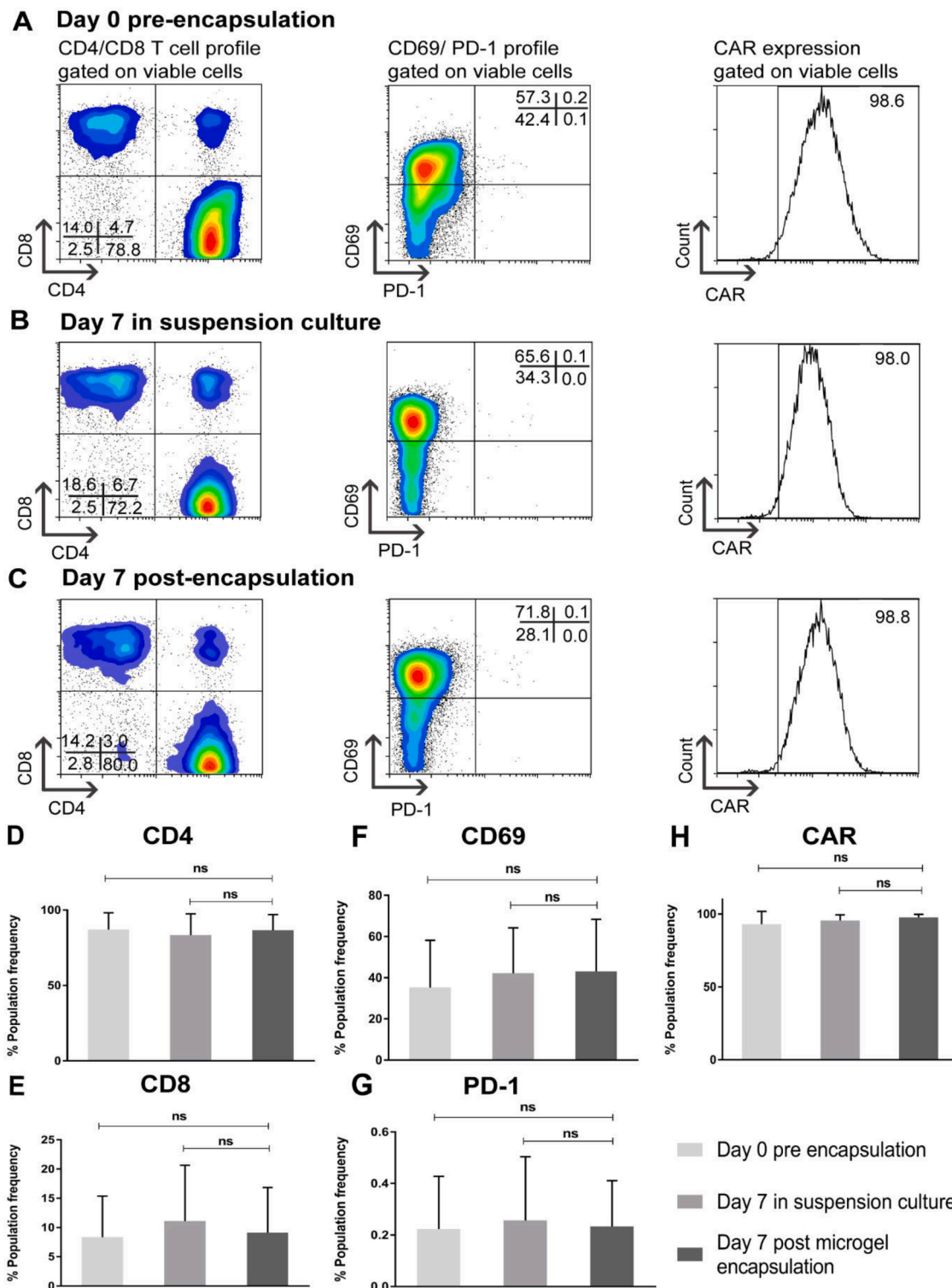


**Fig. 3.** Phenotypic analysis of  $\alpha$ TAG-72 CAR-T cells. (A-C) Representative flow plots of  $\alpha$ TAG-72 CAR-T cell phenotype analysis (A) Before microgel encapsulation. (B) Day 7 control CAR-T cells in suspension culture without encapsulation. (C) Day 7 post encapsulation CAR-T cells recovered from microgel. Cells were gated on intact, single (based on scatter) and viable cells (based on their ability to exclude PI). (D-H) Population frequency of T cell markers. (D, E) T cell subsets (CD4 and CD8), (F) Activation (CD69), (G) Exhaustion (PD-1), (H) CAR expression. Data shown as mean  $\pm$  SD (n = 3). One-way ANOVA with Bartlett's test and Tukey's post hoc test was performed (ns = no statistical difference).  $\alpha$ TAG-72 CAR-T cells: T cells transduced to express anti TAG-72 CARs; PI: propidium iodide.

the most suitable target for  $\alpha$ TAG-72 CAR-T cells in this assay based on the high TAG-72 expression and clear population shift; it is important to appreciate the factors that impact the surface presentation of TAG-72 are not well understood. Expression may fluctuate with various phases of cell cycle and variations in levels can be observed with different cell

passages [43,44]. Only cancer cells with surface expression of TAG-72 at the point of engagement with the CAR-T cells are theoretically able to be killed via the CAR (Fig. 4B). Functional cytotoxic assessment of CAR-T cells on these tumor lines was required to determine the therapeutic effectiveness of  $\alpha$ TAG-72 CAR-T cells.

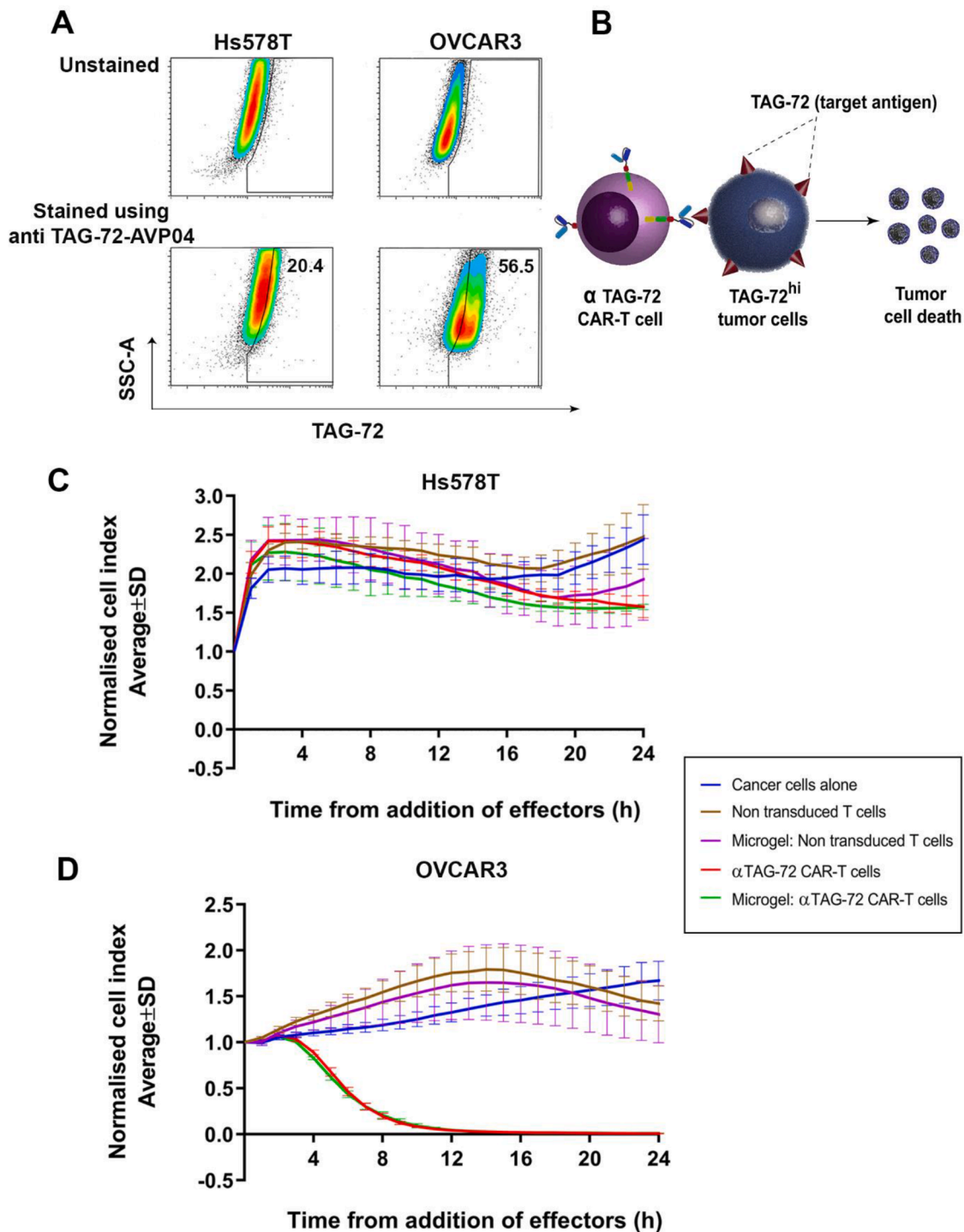


**Fig. 4.** TAG-72 expression in cancer cells and cytotoxicity analysis of  $\alpha$ TAG-72 CAR-T cells (A) Representative flow plots of TAG-72 expression in Hs578T and OVCAR3 cancer cell lines. Cells were gated based on the scatter profiles to identify, single, intact cells with viable cells marked by an absence of PI staining. TAG-72 expression was then gated based on unstained controls (B) Schematic illustration of  $\alpha$ TAG-72 CAR-T cell targeting TAG-72 surface antigens in tumor cells and initiating killing of tumor cells. (C and D) Real-time cytotoxicity analysis of microgel recovered non-transduced T-cells (controls) and  $\alpha$ TAG-72 CAR-T cells using the xCELLigence impedance analysis on target cells at E:T ratio of 5:1 (C) Hs578T and (D) OVCAR3. Data represented as mean  $\pm$  SD for each time point where two independent experiments were conducted with three technical replicates.  $\alpha$ TAG-72 CAR-T cells: T cells transduced to express anti TAG-72 CARs; E:T ratio: effector to target ratio; PI: propidium iodide.

Real-time *in vitro* cytotoxicity analysis revealed that microgel recovered  $\alpha$ TAG-72 CAR-T cells were able to kill TAG-72 expressing OVCAR3 as efficiently as the control CAR-T cells as demonstrated by a reduction in normalized cell index (Fig. 4D). Non-specific killing via NT T cells (no CAR) was not observed, highlighting the potent on-target specificity of the CARs. Functional assessment of CAR-T cells at an E:T

ratio of 1:1 was also investigated demonstrating equivalent findings; microgel encapsulation did not disrupt any on-target recognition or cytotoxic effects against OVCAR-3 compared to CAR-T controls (data not shown). Hs578T cells remained unaffected by the CAR-T cells as they did not show any significant killing with the addition of effector cells (Fig. 4C) which correlates with the lower expression of TAG-72 in

Hs578T cells observed via flow cytometry (Fig. 4A).

Previous studies have investigated the potential of injectable hydrogels for T cell delivery [34,45]. T cells encapsulated in hydrogels after *in vivo* transfer demonstrated gradual cell egression with no signs of inflammation [34]. CAR-T cells, when delivered via a low viscosity hydrogel based on hyaluronic acid and gelatin have shown an improved cytotoxic effect when compared to cells resuspended in saline [45].

Herein, our study demonstrates the potent cytotoxic effect of microgel recovered CAR-T cells on TAG-72 high OVCAR3 suggesting the feasibility of microgels for releasing CAR-T cells without compromising functionality.

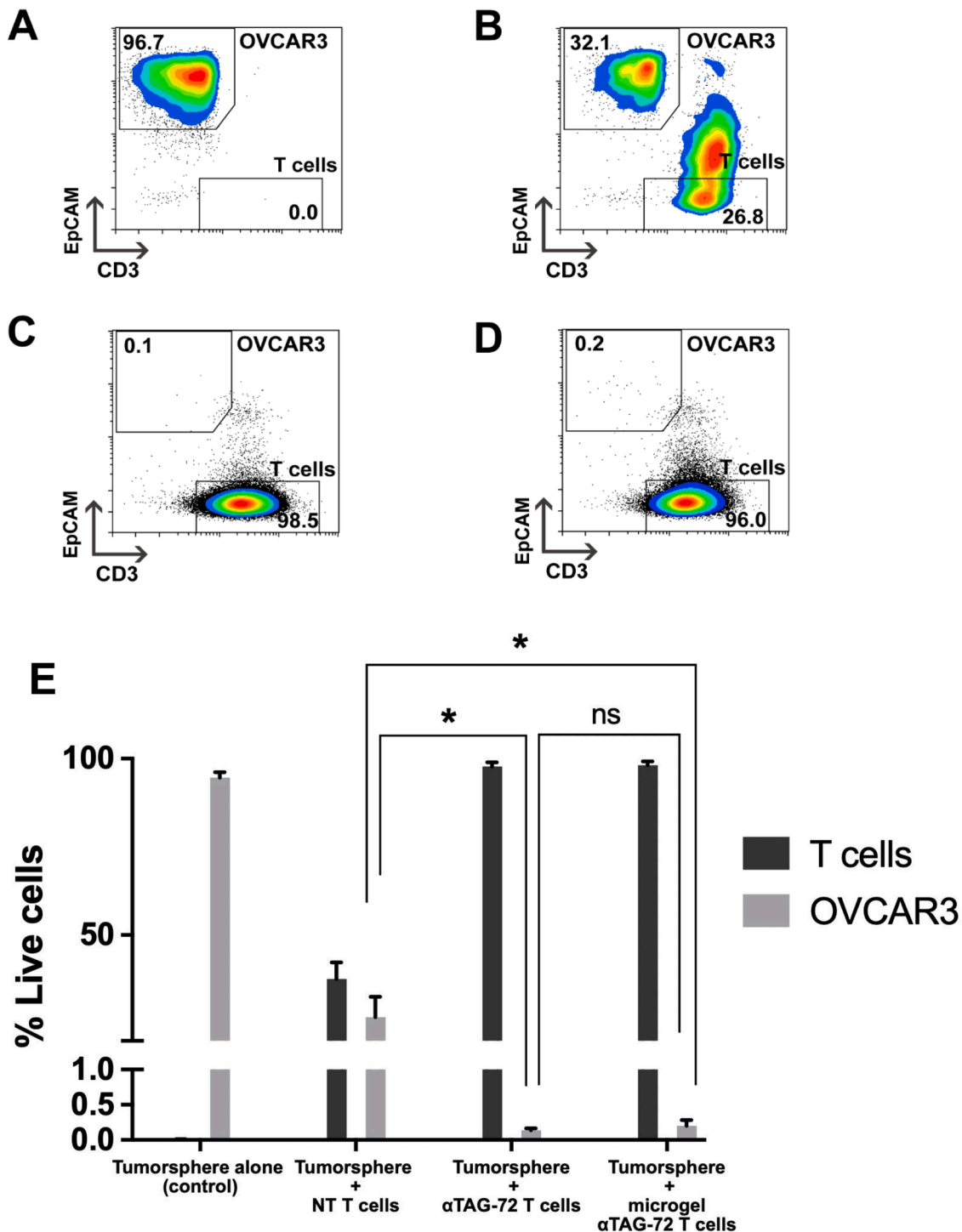


**Fig. 5.** Representative flow cytometric analysis of OVCAR3 spheroids after 4 days of T cell addition (A) tumorsphere control, (B) with non-transduced (NT) T cells (no CAR) (C) with control  $\alpha$ TAG-72 CAR-T cells (D) with microgel recovered  $\alpha$ TAG-72 CAR-T cells. (E) Proportion of live T cells and OVCAR3 after 4 days. Mean  $\pm$  SD is presented (n = 3). Unpaired (nonparametric) t-test with welch's correction was performed assessing percentage of OVCAR3 cells following co-culture with NT T cells compared with  $\alpha$ TAG-72 T cells, NT T cells compared with microgel  $\alpha$ TAG-72 T cells, and  $\alpha$ TAG-72 T cells compared with microgel  $\alpha$ TAG-72 T cells. (ns = no statistical difference, \* $p < 0.05$ ).  $\alpha$ TAG-72 CAR-T cells: T cells transduced to express anti TAG-72 CARs.

### Microgel recovered CAR-T cells destroy 3D ovarian cancer tumorspheres *in vitro*

To study the cytotoxic potential of CAR-T cells, 3D tumor spheroids were generated from OVCAR3 (Fig. S1A). OVCAR3 cells displayed a TFE of  $0.9 \pm 0.2\%$ , TFE indicates the percentage of cells able to form spheroid from a single cell by clonal expansion, a property considered unique to stem-like cells [46]. Tumorsphere cultures are often used to enrich cancer stem cells, which are considered as tumor initiators and the major cause of cancer resistance and relapse [47,48]. Therefore, the use of tumor spheroids in *in vitro* cancer treatment studies could provide a more accurate outcome, bridging the gap between 2D monolayer cultures and animal models.

Cytotoxic functionality of microgel recovered CAR-T cells on OVCAR3 tumorspheres, was demonstrated via live-cell imaging (Fig. S1-3). Tumorsphere controls (Fig. S1A), tumorsphere/NT T cell co-cultures (Fig. S1B) and 2D monolayer/CAR-T cell co-cultures (Fig. S2A) were also studied to support functionality. NT T cells did not affect spheroid morphology (Fig. S1B) which concurred with the NT T cell function in 2D real-time *in vitro* cytotoxicity assays (Fig. 4D). In 2D cancer monolayers/CAR-T cell co-cultures, CAR-T cells degranulated the cancer cells at earlier time points (Fig. S2A) which would be expected based on the 2D *in vitro* cytotoxicity assay (Fig. 4D).

In 3D tumorspheres/CAR-T cell co-cultures, with control CAR-T cells (cells grown in suspension cultures) (Fig. S2B) and microgel recovered CAR-T cells (Fig. S3A, B, Video S4), T cells migration towards cancer cells and subsequent attack were visualized (Fig. S3B, yellow arrow). CAR-T cells degranulated the adherent layer of cells present in the spheroid cultures; however, the 3D spheroid masses were not significantly impacted within the short period (15 h) (Video S4). Unlike 2D monolayers cultures, 3D spheroid masses are inherently more complex; we postulated that CAR-T cells may require extended time periods to elicit a complete cytotoxic response in this setting. Nonetheless, this study has shown the functionality of microgel recovered CAR-T cells, demonstrating these hydrogels are candidate vehicles for delivering CAR-T cells capable of destroying 3D solid tumors.

To analyze the outcome of extended co-cultures, flow cytometric analyses (Fig. 5) were performed after 4 days of the addition of CAR-T cells. Untreated OVCAR3 tumorspheres displayed  $95.6 \pm 1.6\%$  (Fig. 5A, E) expression of EpCAM on live cells in culture, validating the assay and tumor alone controls. With the addition of NT cells (Fig. 5B), whilst the proportion of live OVCAR3 cells was  $26.7 \pm 5.7\%$  (as it was no longer a monoculture of tumor cells alone), the clear population of EpCAM+ OVCAR3 cells indicates survival of the tumor (Fig. 5B, E). CAR-T cells recovered from microgels following enzymatic digestion annihilated 3D spheroid masses with equivalent efficacy compared to control CAR-T cells as shown in Fig. 5C-E. Here we have shown that the encapsulation of CAR-T cells in microgels does not impact the cytotoxic function of CARs and encapsulated cells demonstrated functional equivalence. The benefit of microgels for enabling sustained delivery of CAR-T cells at the tumor site has to be analyzed via *in vivo* studies.

The optimized microgel encapsulation conditions utilized in this study provide a plausible system for CAR-T cell encapsulation, and application demonstration against 3D ovarian tumor spheroids. With the assurance of potent on-target CAR-T function, the micro-hydrogel manufacture system provides a suitable platform to investigate potential advantages *in vivo* and characterization of prolonged CAR-T release at the tumor site, for example using in an intraperitoneal injection into ovarian tumor model in NGS mice.

### Conclusion

This study demonstrates the feasibility of gelatin-based microgels as carrier systems to deliver CAR-T cells that retain potent cytotoxic function against ovarian cancer *in vitro*.  $\alpha$ TAG-72 CAR-T cells encapsulated within microgels showed more than 87% viability on day 7 post-

encapsulation. *In vitro* studies show that the recovered CAR-T cells maintain their phenotype and ability to kill TAG-72 expressing ovarian cancer cell line, OVCAR3. Live cell imaging and flow cytometry of OVCAR3 tumorsphere co-cultures with  $\alpha$ TAG-72 CAR-T cells revealed the capability of these microgels as cell delivery vehicles for CAR-T cells by completely removing 3D solid ovarian tumors *in vitro*. This study provides proof of concept evidence showing the feasibility of microgels as delivery vehicles of CAR-T cells targeting ovarian cancer cells. *In vivo* studies in humanized mice models are a logical and exciting next step to further establish these *in vitro* findings.

### Supporting Information

Synthesis of gelatin norbornene (GelNB); Table S1. Antibodies utilized for  $\alpha$ TAG-72 CAR-T cells phenotype analysis; Table S2. Antibodies utilized for FACS analysis of spheroids and CAR-T cells; Fig. S1. Time-lapse images of OVCAR3 spheroids; Fig. S2. Time-lapse images of  $\alpha$ TAG-72 CAR-T cells attacking OVCAR3 spheroids; Fig. S3. Time-lapse images of microgel recovered  $\alpha$ TAG-72 CAR-T cells attacking OVCAR3 tumorspheres; Video S4. Real-time live-cell imaging of microgel recovered  $\alpha$ TAG-72 CAR-T cells attacking OVCAR3 cells and spheroids.

### CRediT authorship contribution statement

**Anisha B. Suraiya:** Investigation, Methodology, Data curation, Formal analysis, Writing – original draft, Writing – review & editing. **Vera J. Evtimov:** Investigation, Methodology, Writing – review & editing. **Vinh X. Truong:** Methodology, Writing – review & editing. **Richard L. Boyd:** Conceptualization, Supervision, Funding acquisition, Writing – review & editing. **John S. Forsythe:** Conceptualization, Supervision, Funding acquisition, Writing – review & editing. **Nicholas R. Boyd:** Conceptualization, Supervision, Investigation, Formal analysis, Funding acquisition, Writing – review & editing.

### Conflict of Interest

V.J.E and N.R.B are employed by Cartherics Pty Ltd and are eligible for equity-based remuneration under the company's employee share option plan. R.L.B is employed by Cartherics Pty Ltd and holds equity in the company.

### Acknowledgments

This study was supported by Cartherics Pty, Ltd, Australia and the Australian Research Council Discovery Project DP160101591 awarded to J.S.F. The authors acknowledge the use of facilities at Monash Micro Imaging (MMI, Monash University) and MMI-Monash Health Translation Precinct (MMI-MHTP). We also thank Dr Sarah Creed (MMI-MHTP) for the help with real-time imaging and analyses. A.B.S acknowledges support from the Australian Government Research Training Program (RTP) Scholarship and CRC-P for Allogeneic Stem Cell Cancer Immunotherapies top-up scholarship.

### Supplementary materials

Supplementary material associated with this article can be found, in the online version, at doi:10.1016/j.tranon.2022.101477.

### References

- [1] A.J. Smith, J. Oertle, D. Warren, D. Prato, Chimeric antigen receptor (CAR) T cell therapy for malignant cancers: Summary and perspective, *J. Cellular Immunother.* 2 (2) (2016) 59–68.
- [2] K. Newick, E. Moon, S.M. Albelda, Chimeric antigen receptor T-cell therapy for solid tumors, *Mol. Ther. - Oncol.* 3 (2016) 16006.
- [3] S.L. Maude, N. Frey, P.A. Shaw, R. Aplenc, D.M. Barrett, N.J. Bunin, A. Chew, V. E. Gonzalez, Z. Zheng, S.F. Lacey, Y.D. Mahnke, J.J. Melenhorst, S.R. Rheingold,

- A. Shen, D.T. Teachey, B.L. Levine, C.H. June, D.L. Porter, S.A. Grupp, Chimeric Antigen Receptor T Cells for Sustained Remissions in Leukemia, *New Engl. J. Med.* 371 (16) (2014) 1507–1517.
- [4] L.-N. Zhang, Y. Song, D. Liu, CD19 CAR-T cell therapy for relapsed/refractory acute lymphoblastic leukemia: factors affecting toxicities and long-term efficacies, *J. Hematol. Oncol.* 11 (1) (2018) 41.
- [5] M. Martinez, E.K. Moon, CAR T Cells for Solid Tumors: New Strategies for Finding, Infiltrating, and Surviving in the Tumor Microenvironment, *Front. Immunol.* 10 (2019) 128.
- [6] K. Renner, K. Singer, G.E. Koehl, E.K. Geissler, K. Peter, P.J. Siska, M. Kreutz, Metabolic Hallmarks of Tumor and Immune Cells in the Tumor Microenvironment. (Report)(Author abstract), *Front. Immunol.* 8 (2017).
- [7] H.M. Knochelmann, A.S. Smith, C.J. Dwyer, M.M. Wyatt, S. Mehrotra, C.M. Paulos, CAR T cells in solid tumors: blueprints for building effective therapies, *Front. Immunol.* 9 (2018) 1740.
- [8] G.M. Konjević, A.M. Vuletić, K.M. Mirjačić Martinović, A.K. Larsen, V.B. Jurišić, The role of cytokines in the regulation of NK cells in the tumor environment, *Cytokine* 117 (2019) 30–40.
- [9] N. Ramamonjisoa, E. Ackerstaff, Characterization of the Tumor Microenvironment and Tumor–Stroma Interaction by Non-invasive Preclinical Imaging, *Front. Oncol.* 7 (2017).
- [10] T.N. Schumacher, R.D. Schreiber, Neoantigens in cancer immunotherapy, *Science* 348 (6230) (2015) 69–74 (New York, N.Y.).
- [11] A. Thor, F. Gorstein, N. Ohuchi, C.A. Szpak, W.W. Johnston, J. Schlom, Tumor-associated glycoprotein (TAG-72) in ovarian carcinomas defined by monoclonal antibody B72.3, *J. Natl. Cancer Inst.* 76 (6) (1986) 995–1006.
- [12] C. Pizzi, A. Sgambato, M. De Laurentiis, G. Limite, L. Panico, G. Pettinato, R. Muraro, L. Tauchmanova, A. Galietta, A.R. Bianco, R. Mariani-Costantini, A. Contegiacomo, TAG-72 expression and clinical outcome in primary breast cancer, *Oncol. Rep.* 6 (6) (1999) 1399–1403.
- [13] P.C. Brenner, W.J. Rettig, P.M. Sanz-Moncasi, V. Reuter, A. Aprikian, L.J. Old, W. R. Fair, P. Garin-Chesa, TAG-72 Expression in Primary, Metastatic and Hormonally Treated Prostate Cancer as Defined by Monoclonal Antibody CC49, *J. Urol.* 153 (5) (1995) 1575–1579.
- [14] M. Xu, F.X. Real, S. Welt, M.H. Schussler, H.F. Oettgen, L.J. Old, Expression of TAG-72 in normal colon, transitional mucosa, and colon cancer, *Int. J. Cancer* 44 (6) (1989) 985–989.
- [15] A. Thor, N. Ohuchi, C.A. Szpak, W.W. Johnston, J. Schlom, Distribution of oncofetal antigen tumor-associated glycoprotein-72 defined by monoclonal antibody B72.3, *Cancer Res* 46 (6) (1986) 3118–3124.
- [16] M.P. Ponnusamy, G. Venkatraman, A.P. Singh, S.C. Chauhan, S.L. Johansson, M. Jain, L. Smith, J.S. Davis, S.W. Remmenga, S.K. Batra, Expression of TAG-72 in ovarian cancer and its correlation with tumor stage and patient prognosis, *Cancer Lett.* 251 (2) (2007) 247–257.
- [17] S.L. Maude, T.W. Laetsch, J. Buechner, S. Rives, M. Boyer, H. Bittencourt, P. Bader, M.R. Verneris, H.E. Stefanski, G.D. Myers, M. Qayed, B. De Moerloose, H. Hiramatsu, K. Schlis, K.L. Davis, P.L. Martin, E.R. Nemecek, G.A. Yanik, C. Peters, A. Baruchel, N. Boissel, F. Melchinaud, A. Balduzzi, J. Krueger, C.H. June, B.L. Levine, P. Wood, T. Taran, M. Leung, K.T. Mueller, Y. Zhang, K. Sen, D. Leibold, M.A. Pulsipher, S.A. Grupp, Tisagenlecleucel in Children and Young Adults with B-Cell Lymphoblastic Leukemia, *N. Engl. J. Med.* 378 (5) (2018) 439–448.
- [18] S.S. Neelapu, F.L. Locke, N.L. Bartlett, L.J. Lekakis, D.B. Miklos, C.A. Jacobson, I. Braunschweig, O.O. Oluwole, T. Siddiqi, Y. Lin, J.M. Timmerman, P.J. Stiff, J. W. Friedberg, I.W. Flinn, A. Goy, B.T. Hill, M.R. Smith, A. Deol, U. Farooq, P. McSweeney, J. Munoz, I. Avivi, J.E. Castro, J.R. Westin, J.C. Chavez, A. Ghobadi, K.V. Komanduri, R. Levy, E.D. Jacobsen, T.E. Witzig, P. Reagan, A. Bot, J. Rossi, L. Navale, Y. Jiang, J. Aycock, M. Elias, S. Chang, J. Wieszorek, W. Y. Go, Axicabtagene Ciloleucel CAR T-Cell Therapy in Refractory Large B-Cell Lymphoma, *N. Engl. J. Med.* 377 (26) (2017) 2531–2544.
- [19] D. Porter, N. Frey, P.A. Wood, Y. Weng, S.A. Grupp, Grading of cytokine release syndrome associated with the CAR T cell therapy tisagenlecleucel, *J. Hematol. Oncol.* 11 (1) (2018) 35.
- [20] T. Giavridis, S.J.C. van der Stegen, J. Eyquem, M. Hamieh, A. Piersigilli, M. Sadelain, CAR T cell-induced cytokine release syndrome is mediated by macrophages and abated by IL-1 blockade, *Nat. Med.* 24 (6) (2018) 731–738.
- [21] V. Jurisic, Multiomic analysis of cytokines in immuno-oncology, *Expert Rev. Proteom.* 17 (9) (2020) 663–674.
- [22] S.B. Stephan, A.M. Taber, I. Jileeva, E.P. Pegues, C.L. Sentman, M.T. Stephan, Biopolymer implants enhance the efficacy of adoptive T-cell therapy, *Nat. Biotechnol.* 33 (2014) 97.
- [23] T.T. Smith, H.F. Moffett, S.B. Stephan, C.F. Opel, A.G. Dumigan, X. Jiang, V. G. Pillarisetty, S.P.S. Pillai, K.D. Witttrup, M.T. Stephan, Biopolymers codelivering engineered T cells and STING agonists can eliminate heterogeneous tumors, *J. Clin. Invest.* 127 (6) (2017) 2176–2191.
- [24] A.B. Suraiya, M.L. Hun, V.X. Truong, J.S. Forsythe, A.P. Chidgey, Gelatin-Based 3D Microgels for In Vitro T Lineage Cell Generation, *ACS Biomater. Sci. Eng.* 6 (4) (2020) 2198–2208.
- [25] F. Li, V.X. Truong, H. Thissen, J.E. Frith, J.S. Forsythe, Microfluidic Encapsulation of Human Mesenchymal Stem Cells for Articular Cartilage Tissue Regeneration, *ACS Appl. Mater. Interfaces* 9 (10) (2017) 8589–8601.
- [26] F. Li, V.X. Truong, P. Fisch, C. Levinson, V. Glattauer, M. Zenobi-Wong, H. Thissen, J.S. Forsythe, J.E. Frith, Cartilage tissue formation through assembly of microgels containing mesenchymal stem cells, *Acta Biomater* 77 (2018) 48–62.
- [27] J.M. Lee, P. Mhawech-Fauceglia, N. Lee, L.C. Parsanian, Y.G. Lin, S.A. Gayther, K. Lawrenson, A three-dimensional microenvironment alters protein expression and chemosensitivity of epithelial ovarian cancer cells in vitro, *Lab. Invest.* 93 (5) (2013) 528–542.
- [28] L.W. Dunne, Z. Huang, W. Meng, X. Fan, N. Zhang, Q. Zhang, Z. An, Human decellularized adipose tissue scaffold as a model for breast cancer cell growth and drug treatments, *Biomaterials* 35 (18) (2014) 4940–4949.
- [29] S. Shrestha, F. Li, V.X. Truong, J.S. Forsythe, J.E. Frith, Interplay of Hydrogel Composition and Geometry on Human Mesenchymal Stem Cell Osteogenesis, *Biomacromolecules* 21 (12) (2020) 5323–5335.
- [30] R. Shu, V.J. Evtimov, M.V. Hammett, N.-Y.N. Nguyen, J. Zhuang, P.J. Hudson, M. C. Howard, A. Pupovac, A.O. Trounson, R.L. Boyd, Engineered CAR-T cells targeting TAG-72 and CD47 in ovarian cancer, *Molecular Therapy - Oncol.* 20 (2021) 325–341.
- [31] G. Dontu, W.M. Abdallah, J.M. Foley, K.W. Jackson, M.F. Clarke, M.J. Kawamura, M.S. Wicha, In vitro propagation and transcriptional profiling of human mammary stem/progenitor cells, *Genes Dev* 17 (10) (2003) 1253–1270.
- [32] J.C. Pease, M. Brewer, J.S. Tirnauer, Spontaneous spheroid budding from monolayers: a potential contribution to ovarian cancer dissemination, *Biology Open* 1 (7) (2012) 622.
- [33] J.W. Hickey, Y. Dong, J.W. Chung, S.F. Salathe, H.C. Pruiett, X. Li, C. Chang, A. K. Fraser, C.A. Bessell, A.J. Ewald, S. Gerecht, H.-Q. Mao, J.P. Schneck, Engineering an Artificial T-Cell Stimulating Matrix for Immunotherapy, *Adv. Mater.* 31 (23) (2019), 1807359.
- [34] J. Weiden, D. Voerman, Y. Dolen, R.K. Das, A. van Duffelen, R. Hammink, L. J. Eggermont, A.E. Rowan, J. Tel. C.G. Figdor, Injectable Biomimetic Hydrogels as Tools for Efficient T Cell Expansion and Delivery, *Front. Immunol.* 9 (2018) 2798.
- [35] D. Cibrián, F. Sánchez-Madrid, CD69: from activation marker to metabolic gatekeeper, *Eur. J. Immunol.* 47 (6) (2017) 946–953.
- [36] Y. Latchman, C.R. Wood, T. Chernova, D. Chaudhary, M. Borde, I. Chernova, Y. Iwai, A.J. Long, J.A. Brown, R. Nunes, E.A. Greenfield, K. Bourque, V. A. Boussiotis, L.L. Carter, B.M. Carreno, N. Malenkovich, H. Nishimura, T. Okazaki, T. Honjo, A.H. Sharpe, G.J. Freeman, PD-L2 is a second ligand for PD-1 and inhibits T cell activation, *Nat. Immunol.* 2 (3) (2001) 261–268.
- [37] A. Amadori, R. Zamarchi, G. De Silvestro, G. Forza, G. Cavatton, G.A. Danieli, M. Clementi, L. Chieco-Bianchi, Genetic control of the CD4/CD8 T-cell ratio in humans, *Nat. Med.* 1 (12) (1995) 1279–1283.
- [38] J. Lee, E. Ahn, H.T. Kissick, R. Ahmed, Reinvigorating Exhausted T Cells by Blockade of the PD-1 Pathway, *For. Immunopathol. Dis. Therap.* 6 (1-2) (2015) 7–17.
- [39] S.C. Chauhan, N. Vinayek, D.M. Maher, M.C. Bell, K.A. Dunham, M.D. Koch, Y. Lio, M. Jaggi, Combined Staining of TAG-72, MUC1, and CA125 Improves Labeling Sensitivity in Ovarian Cancer: Antigens for Multi-targeted Antibody-guided Therapy, *J. Histochem. Cytochem.* 55 (8) (2007) 867–875.
- [40] J.P. Murad, A.K. Kozłowska, H.J. Lee, M. Ramamurthy, W.C. Chang, P. Yazaki, D. Colcher, J. Shively, M. Cristea, S.J. Forman, S.J. Priceman, Effective Targeting of TAG72(+) Peritoneal Ovarian Tumors via Regional Delivery of CAR-Engineered T Cells, *Front. Immunol.* 9 (2018) 2268.
- [41] F.J. Kelly, C.R. Miller, D.J. Buchsbaum, J. Gomez-Navarro, M.N. Barnes, R. D. Alvarez, D.T. Curiel, Selectivity of TAG-72-targeted Adenoviral Gene Transfer to Primary Ovarian Carcinoma Cells & in Vitro & in Vivo, *Autologous Mesothelial Cells & in Vitro & in Vivo*, *Clin. Cancer Res.* 6 (11) (2000) 4323.
- [42] C.M. Nicolet, D.H. Siegel, J.E. Surfus, P.M. Sondag, TAG-72-reactive antibody CC49 recognizes molecules expressed by hematopoietic cell lines, *Tumour Biol.* 18 (6) (1997) 356–366.
- [43] P. Horan Hand, D. Colcher, D. Salomon, J. Ridge, P. Noguchi, J. Schlom, Influence of spatial configuration of carcinoma cell populations on the expression of a tumor-associated glycoprotein, *Cancer Res.* 45 (2) (1985) 833–840.
- [44] P.H. Hand, M. Nuti, D. Colcher, J. Schlom, Definition of antigenic heterogeneity and modulation among human mammary carcinoma cell populations using monoclonal antibodies to tumor-associated antigens, *Cancer Res.* 43 (2) (1983) 728–735.
- [45] A.F. Atik, C.M. Suryadevara, R.M. Schweller, J.L. West, P. Healy, J.E. Herndon II, K.L. Congdon, L. Sanchez-Perez, R.E. McLendon, G.E. Archer, P. Fecci, J. H. Sampson, Hyaluronic acid based low viscosity hydrogel as a novel carrier for Convection Enhanced Delivery of CAR T cells, *J. Clin. Neurosci.* 56 (2018) 163–168.
- [46] L.B. Weiswald, D. Bellet, V. Dangles-Marie, Spherical cancer models in tumor biology, *Neoplasia* 17 (1) (2015) 1–15.
- [47] S.K. Singh, I.D. Clarke, M. Terasaki, V.E. Bonn, C. Hawkins, J. Squire, P.B. Dirks, Identification of a cancer stem cell in human brain tumors, *Cancer Res* 63 (18) (2003) 5821–5828.
- [48] C.-H. Lee, C.-C. Yu, B.-Y. Wang, W.-W. Chang, Tumorsphere as an effective in vitro platform for screening anti-cancer stem cell drugs, *Oncotarget* 7 (2) (2016) 1215–1226.